Chemical Engineering Journal 217 (2013) 475–485

Contents lists available at SciVerse ScienceDirect

Chemical Engineering Journal

journal homepage: www.elsevier.com/locate/cej

Radiation field modeling and optimization of a compact and modular multi-plate photocatalytic reactor (MPPR) for air/water purification by Monte Carlo method

Ana Luisa Loo Zazueta [a,c], Hugo Destaillats [b], Gianluca Li Puma [c,*]

[a] Department of Chemical and Environmental Engineering, University of Nottingham, Nottingham, UK
[b] Indoor Environment Group, Lawrence Berkeley National Laboratory, Berkeley, CA, USA
[c] Environmental Nanocatalysis and Photoreaction Engineering, Department of Chemical Engineering, Loughborough University, Loughborough, UK

HIGHLIGHTS

- Compact modular design of a multiplate photoreactor facilitates scale-up.
- Large irradiated photocatalyst surface area with high photon utilization efficiency.
- Dimensionless parametric optimization of reactor geometry led to optimum design.
- Monte Carlo method applied to determine photon absorption and spatial distribution.
- Optimum design validated experimentally for the oxidation of toluene in humid air.

GRAPHICAL ABSTRACT

Multi-plate photocatalytic reactor with one lamp and reactor performance parameters.

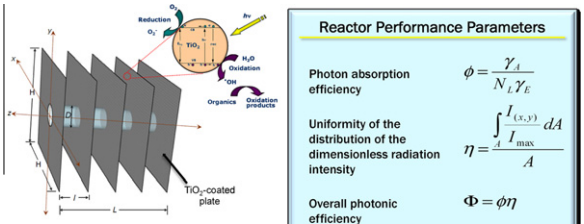

N_L: number of lamps
γ_E: number of photons emitted
γ_A: number of photons absorbed
$I(x,y)$: number of photons striking the differential area dA at the position (x,y)
I_{max}: maximum value of $I(x,y)$
A: total area of a single face plate

ARTICLE INFO

Article history:
Received 20 September 2012
Received in revised form 12 November 2012
Accepted 17 November 2012
Available online 29 November 2012

Keywords:
Photocatalysis
Multi-plate reactor
Monte Carlo simulation
Indoor air
Photoreactor
Water/air treatment

ABSTRACT

The radiation field in a multi-plate photocatalytic reactor (MPPR) for air or water purification was modeled and optimized using a Monte Carlo stochastic method. The MPPR consists of parallel photocatalytic plates irradiated by cylindrical UV lamps orthogonal to the plates. The photocatalyst titanium dioxide (TiO_2) is supported on the plates as a thin film. The photoreactor design is compact and offers a large irradiated photocatalytic surface area, a high degree of photon utilization, low pressure drop and a modular design which can facilitate scale-up. These features are desirable for the decontamination of indoor air in ventilation ducts or for water detoxification. The Monte Carlo method was applied to determine three dimensionless reactor performance parameters: the photon absorption efficiency (ϕ), the uniformity of the distribution of the dimensionless radiation intensity (η) and the overall photonic efficiency (Φ). The emission of photons from the light sources was simulated by the extensive source with superficial emission (ESSE) model. Simulations were performed by varying the catalyst reflectivity albedo, the number and the diameter of lamps, and the dimensions and spacing of the photocatalytic plates. Optimal design for a basic reactor module with one lamp was accomplished for lamp-diameter-to-plate-height ratio (β) of 0.7, while the plate-spacing-to-plate-height ratio (α) was correlated by [$\alpha_{optimum} = 0.191\,\beta^2 - 0.5597\,\beta + 0.3854$]. A multilamp arrangement leads to a feasible increase in the size and number of the plates and the irradiated photocatalytic surface area. The optimum design was validated by measuring the apparent quantum yield of the oxidation of toluene (7 ppmv) in a humidified air stream using immobilized TiO_2 (Degussa P25). Experiments performed varying the geometrical parameter α correlated well with the model calculations, with maximum apparent quantum yield for $\alpha = 0.137$. The results are directly transferable to the treatment of water by photocatalysis.

* Corresponding author. Tel.: +44 (0)1509 222 510; fax: +44 (0)1509 223 923.
E-mail address: g.lipuma@lboro.ac.uk (G. Li Puma).

1385-8947/$ - see front matter © 2012 Elsevier B.V. All rights reserved.
http://dx.doi.org/10.1016/j.cej.2012.11.085

Nomenclature

A	total surface area of the plate (m^2)
c	speed of light in a vacuum (2.997×10^{10} cm s^{-1})
D	diameter of the lamp (m)
h	Plank's constant (6.62×10^{-34} J s)
H	height of the reactor ($H = W$) (m)
I_{max}	maximum value of $I_{(x,y)}$
$I_{(x,y)}$	number of photons striking the differential area dA at the position (x,y)
l	horizontal distance between two contiguous plates (m)
L	length of the reactor equivalent to the length of the lamp (m)
n	number of plates in the reactor
N_A	Avogadro's number (6.023×10^{23} molecules mol^{-1})
N_L	number of lamps
Q	radiant power reaching the TiO_2 film in the photocatalytic reactor (W)
r_o	initial rate of pollutant photoconversion (mol $gcat^{-1}$ s)
W	width of the reactor ($W = H$)
W_{cat}	total weight of catalyst (g)

Greek symbols

α	space between plates to plate height ratio
β	lamp diameter to plate height ratio for one lamp reactor configurations
β'	lamp diameter to plate height ratio for multi-lamp reactor configurations
γ	reactor width to height ratio
γ_A	number of photons absorbed by the plates surface
γ_E	number of photons emitted by each lamp
η	the uniformity of the distribution of the dimensionless radiation intensity
λ	wavelength (m)
ρ	reflectivity albedo
ϕ	photon absorption efficiency
Φ	overall photonic efficiency

1. Introduction

In the past decades, air pollution control has focused on the outdoor environment as it is well known that outdoor air pollution can have adverse effect on human health. However, later studies showed that in many cases levels of pollutants in indoor air and, consequently, risks to health, can be considerably higher than those found outdoors [1].

There are countless sources of pollution in confined environments. These include aerosols, cleaning products, building materials, furniture, carpets, office machines and many others. Even the most common everyday equipment could represent an air pollution source, such as computers which emits 100–200 μg h^{-1} $unit^{-1}$ of volatile organic compounds (VOCs) [2]. Poor indoor air quality influences the occurrence of infectious respiratory illnesses, asthma and allergy symptoms, sick building symptoms, and reduced worker productivity [3]. Fisk and Rosenfeld [4] estimated that the total annual cost of poor indoor air quality is around $100 billion in the U.S.

Indoor air pollution is a persistent problem found not only in buildings but also in transportation vehicles, aircrafts and many other confined spaces. Photocatalytic air cleaning devices, in combination with source control and ventilation appears to be a promising method to reduce VOCs levels, which are among the most abundant indoor air pollutants. Photocatalytic oxidation (PCO) offers several advantages over conventional air purification techniques [5] such as oxidization of low concentration pollutants, ambient temperature and pressure operation, low power consumption, low maintenance requirements, and possibility of use in conjunction with heating, ventilation and air conditioning systems (HVACs) systems. Hence, in recent years, numerous photocatalytic reactors for indoor air cleaning have been studied, including annular [6,7], fixed bed [8,9], flat-plate [10–12], fluidized-bed [13,14], honeycomb [15,16], and optical fiber [17–19]. A major challenge this technology faces, apart issues related to catalyst activity, is a poor catalyst illumination efficiency [20]. In general, effective photon utilization is a critical factor in determining the economic feasibility of a particular photocatalytic reactor design. A deficient use of light within a photocatalytic reactor will inherently lead to high operational costs, which in turn, could prevent the reactor to be implemented especially in cases in which catalyst activity is low. Consequently, the analysis of the radiation field in photocatalytic reactors is an essential step towards the optimization of photocatalytic air cleaners.

The radiation field in a multi-plate reactor can be obtained by solving the radiative transfer equation (RTE). There are several techniques to solve the RTE, including: flux, zone, Monte Carlo and hybrids methods. The mentioned approaches give equal solutions in most cases, however, they attach different degrees of difficulty. Pareek et al. [21] have summarized the various methods developed for solving the RTE.

The Monte Carlo method present several advantages in comparison with other methods, such as the fact that it is relatively simple, it has been successfully used for multiple reactor geometries and it can be employed for reactors of complex geometry. This statistical method is based on following the probable path of discrete bundles of photons until their final fate (absorption or escape from the reactor) is established. To have some statistical significance, a significant sample of photons must be defined.

This study focuses on the analysis and optimization of the geometry and radiation field in a multi-plate photocatalytic reactor (MPPR) irradiated by cylindrical UV lamps orthogonal to the plates, a reactor virtually not studied before. The reactor offers a very compact design which can be used for both water and air purification with the catalyst immobilized on the plates. The literature presents only a brief study on a similar reactor irradiated by solar light [22]. The MPPR aims to provide not only high light utilization, but also low pressure drop which is particularly important in HVACs treating large volumes of air. The MPPR presents a large photocatalyst surface area as well as a modular design, which facilitates scale up and retrofitting of current HVAC systems in buildings. The lightweight and compact design also may be suitable for installation in aircraft air purification systems. All these characteristics could make the MPPR a cost-effective alternative for indoor air remediation or water purification. The optimum design was validated by the oxidation of toluene in a humidified air stream.

2. Reactor design

The multi-plate photocatalytic reactor consists of a number of parallel and closely spaced aluminum plates. The plates are perfect squares (or rectangles) coated with TiO_2 films whilst the lamps are inserted perpendicularly to them. Fig. 1 shows a possible reactor configuration with one lamp and a square configuration. This reactor structure provides an efficient contact of photons, solid catalyst and reactants. A small pitch between plates is desired to increase

the catalyst surface area exposed to reactant and photons. The transversal dimensions of the reactor should be selected considering the design stream flowrate aiming to operation under turbulent flow conditions which favor the diffusion and convective transport of pollutants towards the catalytic surface. Furthermore, the contact time (space time) between the pollutants and the catalyst can be increased by connecting optimized MPPR modules in series to provide the desired conversion of reactants and degradation products. In contrast to monolith photocatalytic reactor configurations utilizing UV lamps in between monoliths [14,15] in which a significant fraction of radiation does not reach the monoliths, the MPPR offers a much higher degree of photon utilization if it is designed in such a way to avoid significant photon losses to the inactive reactor walls. Therefore, the size of the photocatalytic plates with respect to the light source and the number of plates fitted in the reactor should be optimized to avoid excessive losses of photons. In such a way an optimal design of the MPPR can be realized.

Two dimensionless geometric ratios are introduced to model the geometry of the reactor:

$$\alpha = l/H \tag{1}$$

$$\beta = D/H \tag{2}$$

where l is the horizontal distance between two contiguous plates, D is the diameter of the lamp and H is the height of the reactor plates. The number of plates in the reactor can be calculated from:

$$n = L/l + 1 \tag{3}$$

where L is the length of the reactor equivalent to the length of the lamp.

For multi-lamp reactors, the lamps can be arranged inline (Fig. 2a) or staggered (Fig. 2b). In order to facilitate comparison of results, the plates are divided into smaller sections; these sections circumscribe each of the lamps in the reactor. And, its dimensions are given by the shortest distance between the centerline of two contiguous lamps. In the case of the reactor with an inline arrangement, the section size can be defined by either the longitudinal pitch (S_L) or the transverse pitch (S_T) as they have the same magnitude. On the other hand, in the staggered configuration it can be described by the diagonal pitch (S_D). A new geometric ratio δ, is defined as follows:

$$\delta = S/H \tag{4}$$

where S is the longitudinal pitch for inline arrangements or the diagonal pith for staggered arrangements.

In addition, the geometric ratio β is substituted by a modified geometric ratio β':

$$\beta' = \beta/\delta \tag{5}$$

3. Reactor performance parameters

The aim of this study is to provide a systematic approach for the optimization of the reactor design parameters that results in a high degree of photon utilization and the most uniform distribution of photons over the catalytic plates. The objective here is that the majority of photons should be captured within the reactor boundaries while providing the most uniform irradiation of the photocatalytic surface. From a qualitative point of view, as α decreases and β increases, the distribution of photons on the reactor plates becomes less uniform, while the absorption of photons by the reactor plates is enhanced.

To provide a quantitative analysis to the optimization of the MPPR, three reactor performance parameters, defined previously by Singh et al. [25] for a monolith reactor and now adapted for a multi-plate reactor, were implemented. The first is the "photon absorption efficiency" (ϕ) defined as:

$$\phi = \frac{\gamma_A}{N_L \gamma_E} \tag{6}$$

where γ_A is the number of photons absorbed by the plates surface, γ_E is the number of photons emitted by each lamp, N_L is the number of lamps.

To simplify the simulation process, only the surface area of the reactor plates was considered to be photocatalytically active. Hence, the reactor walls surrounding the plates are assumed to act as a black body that absorbs photons without reflection or photocatalytic activity.

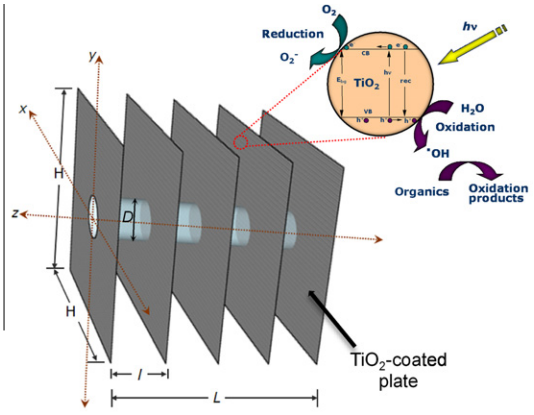

Reactor Performance Parameters

Photon absorption efficiency	$\phi = \frac{\gamma_A}{N_L \gamma_E}$
Uniformity of the distribution of the dimensionless radiation intensity	$\eta = \frac{\int_A \frac{I_{(x,y)}}{I_{max}} dA}{A}$
Overall photonic efficiency	$\Phi = \phi\eta$

N_L: number of lamps

γ_E: number of photons emitted

γ_A: number of photons absorbed

$I(x,y)$: number of photons striking the differential area dA at the position (x,y)

I_{max}: maximum value of $I(x,y)$

A: total area of a single face plate

Fig. 1. Multi-plate photocatalytic reactor with one lamp and reactor performance parameters.

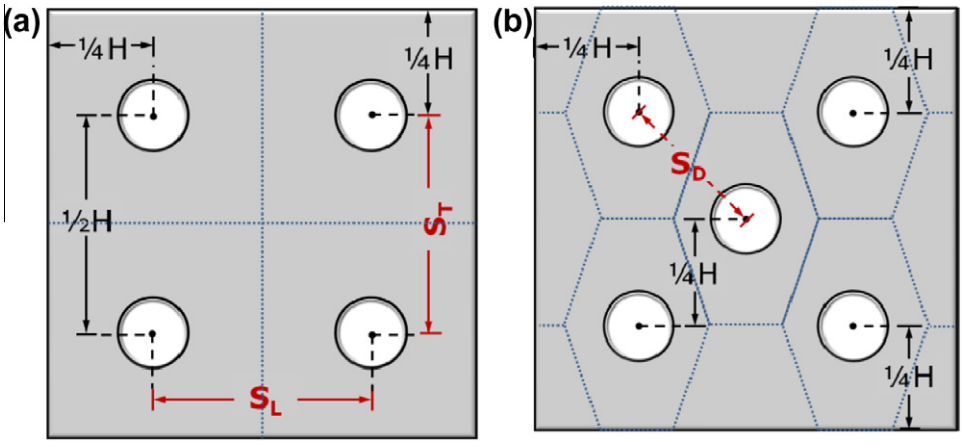

Fig. 2. Reactor plates with multi-lamp configuration: (a) inline arrangement, (b) staggered arrangement.

The second reactor performance parameter is the "uniformity of the distribution of the dimensionless radiation intensity" (η) defined as:

$$\eta = \frac{\int_A \frac{I_{(x,y)}}{I_{max}} dA}{A} \quad (7)$$

where $I_{(x,y)}$ is the number of photons striking the differential area dA at the position (x,y) on the plate surface, I_{max} is the maximum value of $I_{(x,y)}$ and A is the total surface area.

The previous two reactor performance parameters are equally significant since both can influence the extent of pollutant decomposition in the reactor. The first is associated to the absorption of photons and therefore to the rate of photocatalytic decomposition of the pollutant. The second parameter reflects the need to have a uniform irradiation of the plates if photons have to be used efficiently. Hence, the most efficient reactor design should be obtained when the product of ϕ and η reaches a maximum. A third performance indicator, the "overall photonic efficiency" (Φ) can then be defined as:

$$\Phi = \phi\eta \quad (8)$$

Note that the above parameters takes values between 0 and 1 with numbers approaching 1 giving the most efficient reactor configuration.

3.1. Simulation assumptions

(1) Photons are emitted isotropically from the lamp surface following the extensive source with superficial emission model [23] which considers the lamps as a perfect cylinder whose surface emit radiation uniformly. Such assumption is valid for the central portion of fluorescent low-pressure mercury lamps such as blacklights.
(2) The light interaction with the gas (absorption, scattering, and reflection) is ignored.
(3) The absorbance and reflectance of the photocatalytic thin film are independent of light wavelength, light incident angle and thickness of the photocatalytic coating.
(4) The light reflection is perfectly diffuse.
(5) The thin film does not emit radiation in the spectral region of interest.
(6) The photocatalytic thin film coating on the plates is uniform and sufficiently thick such that no catalyst band-gap photons can be transmitted through the thin film. Consequently, band-gap photons can only be absorbed or scattered.
(7) The emitted photon that re-encounters a lamp bulb is absorbed and a new photon is re-emitted.
(8) Photons that strike the non-catalytic reactor walls are assumed to be absorbed (inactive photons) and consequently are lost from the system. Hence, the reflectivity of non-catalytic surfaces is nil.
(9) All the processes taking place in the lamp, such as emission, absorption, and re-emission are at steady state.
(10) Reflection and refraction on the glass envelope of the lamp are ignored.

3.2. Monte Carlo methodology

The Monte Carlo algorithm (Fig. 3) was used as a tool to solve the radiation transfer equation for the dimensionless reactor shown in Fig. 1, to provide quantitative answers to the optimization of the radiation field in a MPPR. This stochastic method consists in tracking each photon emitted by the light source until its final fate: either absorption at the reactor photocatalytic plates surface, or its disappearance on the surroundings (see Fig. 3).

Firstly, a photon is emitted by the UV source. Three random numbers are generated to determine the coordinates of the emission point contained within the surface of the lamp. Subsequently, two additional random numbers define the direction of the photon. The fate of the photon is then calculated. The photon can either hit a reactor wall or the surface of the photocatalytic plate. If the photon hit the reactor wall it will be considered as lost and a new photon is generated. If the photon hits a photocatalytic plate, its location is recorded and a new random number ξ, in the domain from 0 to 1, is generated. If ξ is higher than the reflectivity albedo (ρ) of the photocatalytic thin film, then the photon is absorbed and the count of absorbed photons is increased by one. If $\xi < \rho$, the photon is scattered and a new direction for the reflected photon is determined based on two random numbers. The sequence is repeated until the photon is either absorbed or lost. If a photon hits a lamp, the photon is re-emitted. Finally, the photon absorption efficiency (ϕ) is calculated by dividing the number of photons absorbed by the number of photons emitted by the lamps. In order to determine the uniformity of the distribution of the dimensionless radiation intensity, the surface of the reactor plates is divided in a discrete number of small domains of area dA. The number of photons hitting each domain is calculated from the recorded positions of the photons. Then, Eq. (7) is applied. The simulation is completed by tracking 10^6 photons emitted from each lamp (γ_E) which resulted in the invariability of the results. All simulations were developed in Visual Basic 2008 and Matlab 2007.

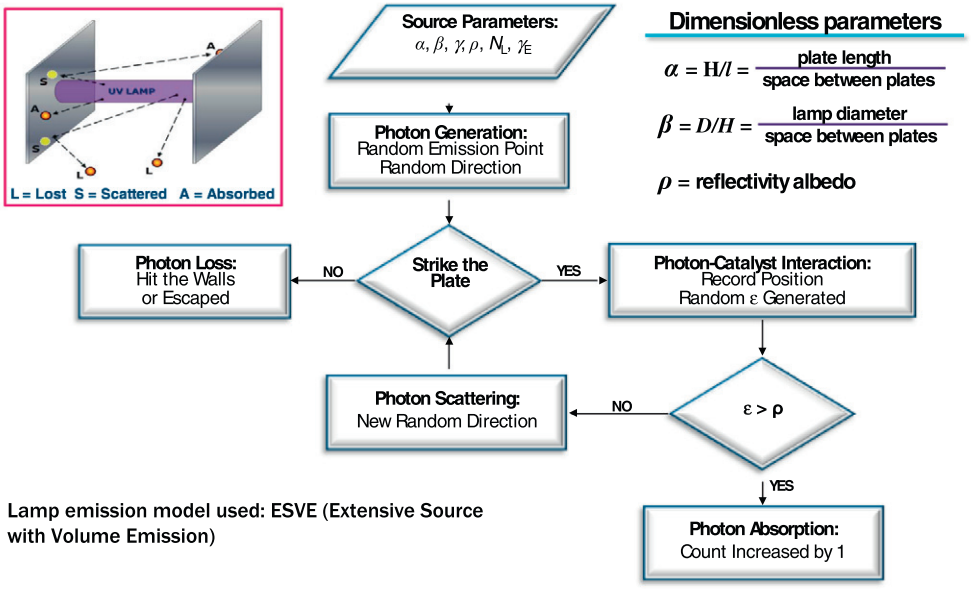

Fig. 3. Monte Carlo algorithm flow chart and fate of photons between two photocatalytic plates.

4. Materials and methods

4.1. Photocatalytic plates, experimental set-up and photocatalytic evaluation

TiO_2 thin films were deposited on square aluminum plates (18.2 cm side length, 2 mm thickness) by dip-coating from a sonicated suspension of TiO_2 (7 wt.%, Degussa P-25; primary particle size, 20–30 nm by TEM; specific surface area 52 $m^2\ g^{-1}$ by BET; composition 78% anatase and 22% rutile by X-ray diffraction) in anhydrous ethanol and polyethylene glycol (PEG 4000, 7 wt.%, Aldrich). The plates were thoroughly cleaned with ethanol and deionized water before coating. The plates were dipped into the suspension and withdrawn at a constant speed of 12 cm min^{-1} using a custom made dip-coating apparatus for large plates. The coating procedure was repeated 8 times with 5 min air drying between the dipping cycles. At the end the plates were air dried for one-hour and further calcined at 520 °C for 90 min in a furnace to obtain visually uniform films. The amount of TiO_2 deposited on the plates determined gravimetrically by the difference of the weight of the plates before and after the coating was 0.5 mg cm^{-2}.

For the purpose of validating the present model two TiO_2-coated plates were mounted in the MPPR at variables distance to achieve different values of the parameter α. Five blacklights lamps (GE T5-F8 W/BLB) were mounted perpendicular to the plates inside quartz lamp sleeves. The emission of radiation from the lamp ends was impeded by Teflon tape for the section protruding over the faces of the plates. In this way only the two facing sides of the two plates were irradiated with photons.

The MPPR was mounted in an air recirculation loop fitted with temperature, pressure and relative humidity sensors, mass flow controllers and a centrifugal fan (Fig. 4). The system was monitored by a computer and a data acquisition device (National Instruments NI USB-6009 and LabVIEW software). The total volume of the reactor and circulation loop was 0.1 m^3.

Ambient air (45% relative humidity and 22 °C) with toluene (anhydrous, 99.8% from Aldrich, 7 ppmv) was circulated in the system at a flowrate of 254 $m^3\ h^{-1}$. Air velocity across the reactor plates was approximately 2.2 m s^{-1}. The pollutant was injected in the recirculation reactor in liquid phase using a microsyringe. The lamps were switched on after an equilibration time of 3 h (Fig. 5). Toluene concentration was higher than levels of total volatile organic compounds (VOCs) typically found indoors, but by no more than one order of magnitude. Hence, these experimental conditions still correspond to the linear Langmuir regime for the adsorption of toluene on TiO_2, and results can be used to predict the performance of the system at lower concentrations. While adsorption of toluene will be affected by the concentration of water vapor in the air (i.e., relative humidity) and by the hydrophilicity of the TiO_2 surface, those two factors are kept constant throughout the experiments and contributing to an "effective" linear Langmuir regime [24]. The flow regime in the reactor was highly turbulent (Reynolds number of 26,000) as a result mass transfer did not limit toluene photodegradation.

The concentration of toluene in the air stream was measured by solid-phase micro extraction (Supelco, 75 m carboxen/PDMS) and GC–MS analysis. The fibers were exposed to the air stream through a septum for 10 s and injected in a Agilent Technologies 6890 N gas chromatograph equipped with a mass selective detector 5975C (DB-VRX column, 20 m, 0.18 mm, 1 micron, 280 °C inlet temperature, 250 °C detector temperature with helium carrier gas and a temperature gradient of 6 °C min^{-1} from 60 to 180 °C). Quantification was performed using a calibration curve in the toluene concentration range from 0.4 to 15 ppmv. A typical toluene concentration profile in the reactor during the equilibration transient time and after irradiation was started (at time = 0) is shown in Fig. 5.

4.2. Experimental evaluation of photon absorption efficiency

A microprocessor controlled radiometer (Cole-Parmer, Model Nr 97503-00) fitted with a 365 nm sensor (bandwidth 355–375 nm) was used for measuring photon fluxes. All UV measurements refer to the bandwidth interval of the sensor.

The photon absorption efficiency was estimated from a radiation balance of the reactor by dividing the radiant power absorbed by the photocatalytic plates by the radiant power emitted by the lamps.

The radiant power emitted by the lamps was estimated by measuring the irradiance at the lamp wall at various longitudinal and

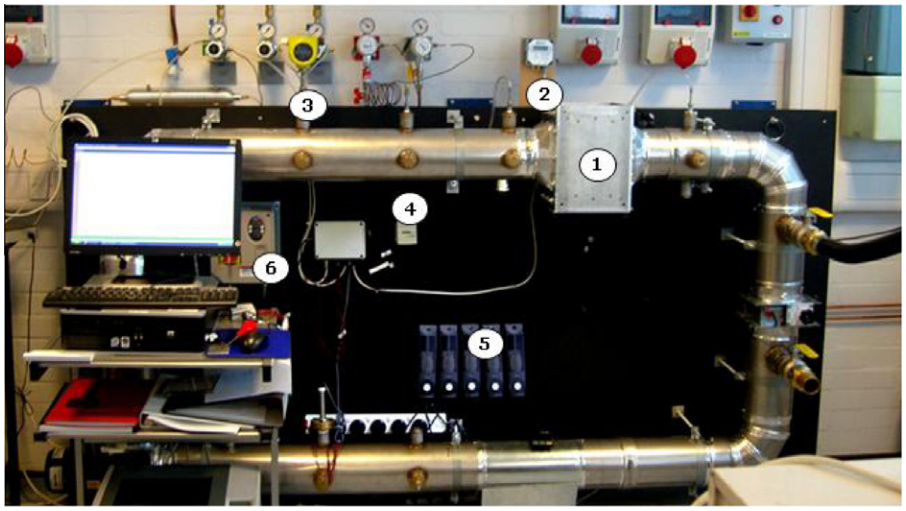

Fig. 4. Experimental set-up: (1) multi-plate photocatalytic reactor, (2) differential pressure sensor, (3) mass flow meter, (4) DAQ device, (5) lamp controllers, (6) fan speed controller.

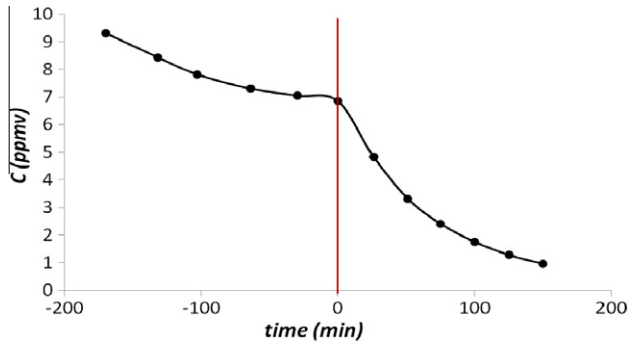

Fig. 5. Typical toluene concentration profile (plates spacing = 17.2 cm).

circumferential locations and integrating over the surface area of the lamp. The radiant power absorbed by the photocatalytic plates was calculated by subtracting the radiant power emitted by the lamp and the radiant power escaping the reactor side walls. This last quantity was computed by measuring the irradiance at the reactor side walls at various locations and integrating over the surface. These considerations assumes that the uncoated reactor walls do not scatter photons and that the TiO_2 coating is sufficiently thick that no photons could be transmitted through the TiO_2 layer.

5. Results and discussion

5.1. Catalyst reflectivity

The catalyst reflectivity (ρ) is defined as the ratio of the reflected to the incident photons. If ρ is equal to 1, all incident photons are scattered. On the contrary, if it is zero, all photons are absorbed by the photocatalytic plates.

TiO_2 photocatalytic thin films tend to have reflectivity values in the range of 0.3 and 0.6, depending on its crystal composition, particle size and surface roughness [25].

In order to approximate the value of the reflectivity in the photocatalytic plates employed in this work, the photon absorption efficiency using values of reflectivity from 0.2 to 0.8 and α from 0.1 to 1 was first calculated through simulations and then compared with the one determined from radiation intensity measurements in the reactor.

Fig. 6 shows a best fitting of the experimental data at $\rho = 0.4$, which is within the range of typical reflectivity values mentioned earlier. Thus, this catalyst film reflectivity was used in further reactor optimization.

Fig. 6 also shows the influence of the reflectivity albedo (ρ) on the photon absorption efficiency when α is varying and β is kept constant. As expected, the photon absorption efficiency decreases as ρ augments. That is, the highest ϕ value is reached when the photocatalytic coating has low reflectivity.

5.2. Geometric ratios

The distribution of the incident radiation over the photocatalytic plates of the reactor is dependent on the separation between them, the diameter of the lamp and the thin-film reflectivity. With the purpose of investigating the effect of the geometrical paramters α and β (Eqs. (1) and (2)) over the reactor performance parameters defined in Section 3, values of α in the range from 0.01 to 1 and of β in the range from 0.2 to 0.8 were considered, while the reflectivity albedo was set to 0.4. Fig. 7a shows the simulation results of the photon absorption efficiency ϕ as a function of β at different values of the geometric parameter α for the reactor configuration with one lamp. ϕ decreases as the plates spacing to plate height ratio increases. When the distance between plates increases, the path length of the photons augments, and so do the number of photons escaping from the reactor. In addition, ϕ is evidently improved by using low lamp diameter to plate height ratios. Clearly, if the diameter of the lamp is small compared to the surface area of the plate, fewer photons will be lost in the surroundings, increasing in this way the number of photons absorbed on the plate.

Fig. 7b and c shows the effect of the modified geometric ratio β' on the photon absorption efficiency for multi-lamp configurations using values of α from 0.2 to 1. Analogously to the case of the reactor with a single lamp, photon absorption efficiency decreases as lamp diameter to plate height ratio augments and it increases as plates spacing to plate height ratio diminishes. Also, as previously determined with the reactor with one lamp, the photon absorption efficiency falls markedly from β' of approximately 0.7. Thus, the geometric parameter β should be selected under 0.7 for optimum design.

It is important to note that the configuration with five lamps displays slightly higher photon absorption efficiency compared to

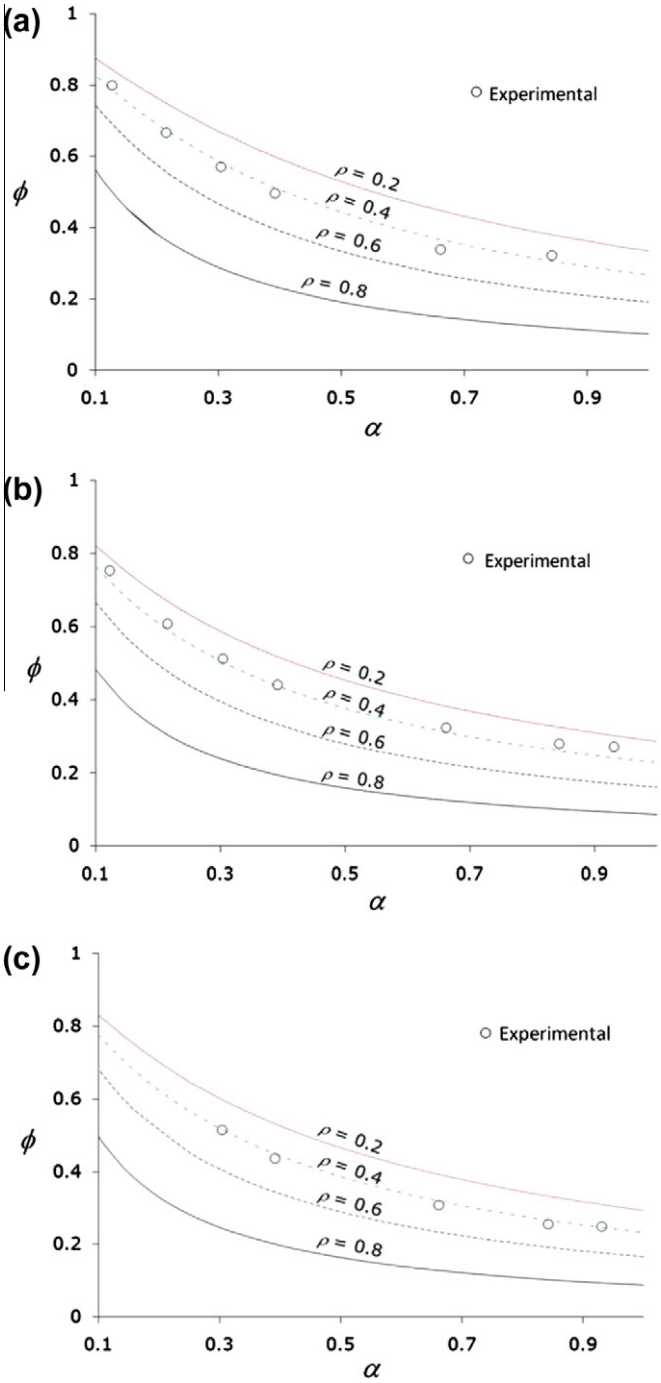

Fig. 6. Comparison of the measured and simulated photon absorption efficiency for the reactor configuration with (a) 1 lamp, (b) 4 lamps and (c) 5 lamps.

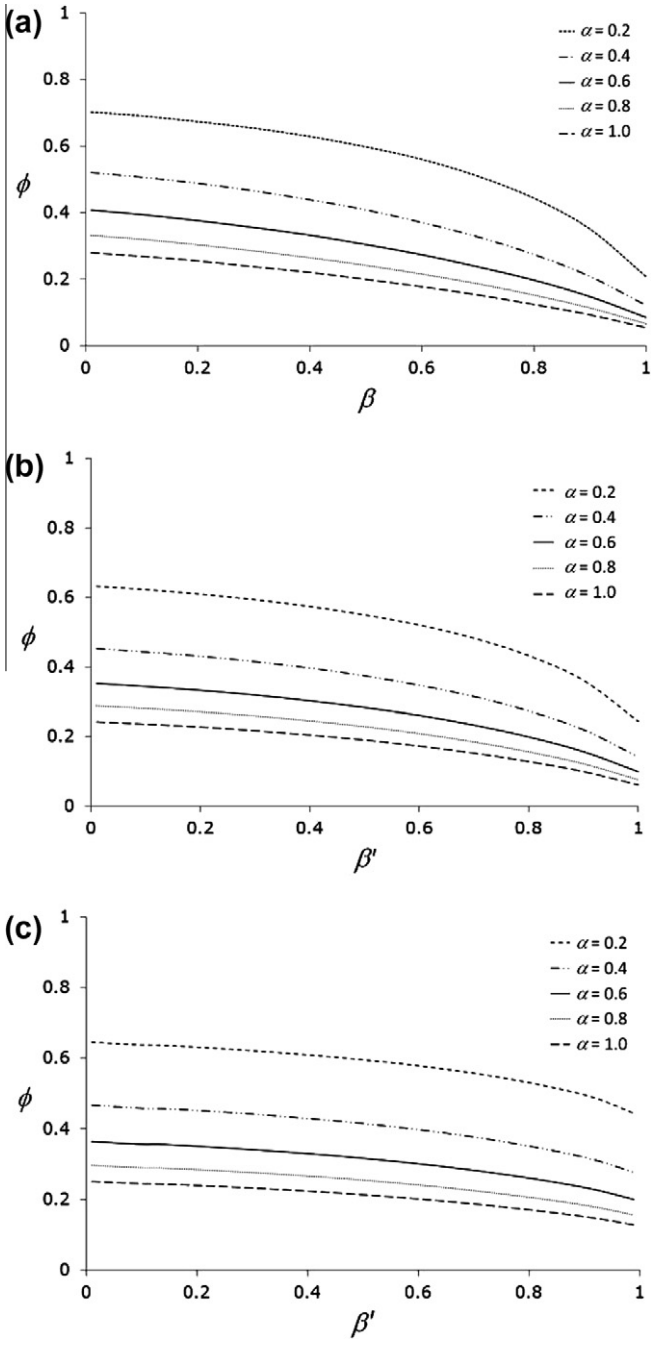

Fig. 7. Influence of α and β on the photon absorption efficiency (ϕ) for the reactor configuration with (a) 1 lamp, (b) 4 lamps and (c) 5 lamps. $\rho = 0.4$.

the one or four lamps. This indicates that the staggered arrangement of lamps is more advantageous in terms of efficiency of photons absorption.

The uniformity of the radiation distribution η over the photocatalytic plates is expected to improve when multiple lamps are used. In addition, this performance parameter is believed to be strongly dependent on the lamps arrangement. Fig. 8 shows the Monte-Carlo simulation results of η at the reactor plate surface when α and β were varied for the reactor configurations with one, four and five lamps. It can be observed that in all the cases, η increases as β and α augment. However, the three plots show significant differences. The uniformity of the radiation distribution for the reactor with one lamp appeared to increase indefinitely as the radius of the lamps augments. Essentially, an increment in the lamp radius leads to a reduction on the surface area surrounding the lamp. And since the light intensity on the photocatalytic surface varies radially, the gradient decreases when the surface area contracts.

In the reactor configuration with four lamps, the gradient of η seems to decrease after β' reaches 0.6. This behavior is the result of having multiple lamps. Photons that would escape in reactors with one lamp might hit instead the surroundings of a different lamp in multi-lamp configurations affecting in this way the distribution of photons on the surface of the plates. Thus, values of β' around 0.6 would be desirable in the case of in-line arrangements

which would give a high uniformity of the radiation distribution while keeping the photocatalytic surface area to a maximum.

Finally, in the case of the reactor with 5 lamps (staggered configuration), η increases rapidly from $\beta' = 0.3$ and then the slope markedly decreases from $\beta' = 0.4$. After this point, the uniformity of the radiation distribution increases slowly and has a second gradient change at $\beta' = 0.7$ from which η maintains nearly constant value. The peculiarities of this configuration are due to the disproportionate distances between lamps along the x and y axes. As β' increases, some regions of the plates surface area (e.g. along the diagonal distance between lamps) are irradiated by photons from multiple lamps, while other regions are irradiated by one lamp only.

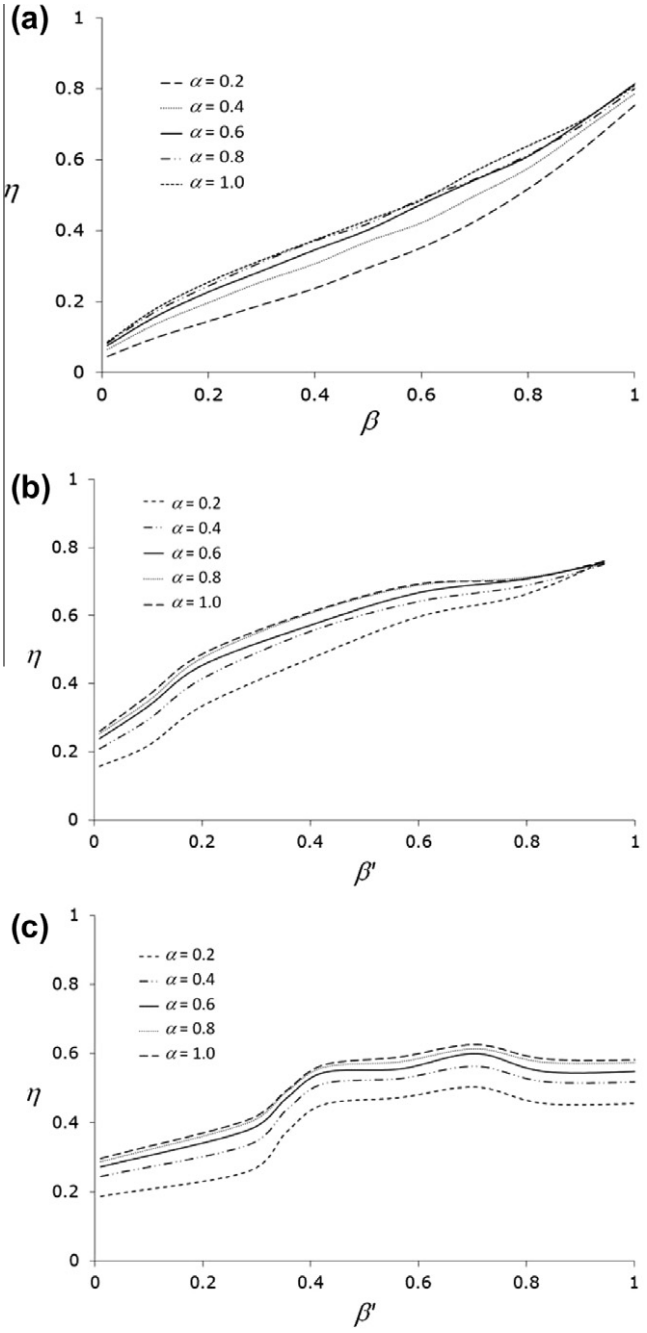

Fig. 8. Influence of α and β on the uniformity of the distribution of the dimensionless radiation intensity ()for the reactor configuration with (a) 1 lamp, (b) 4 lamps and (c) 5 lamps. $\rho = 0.4$.

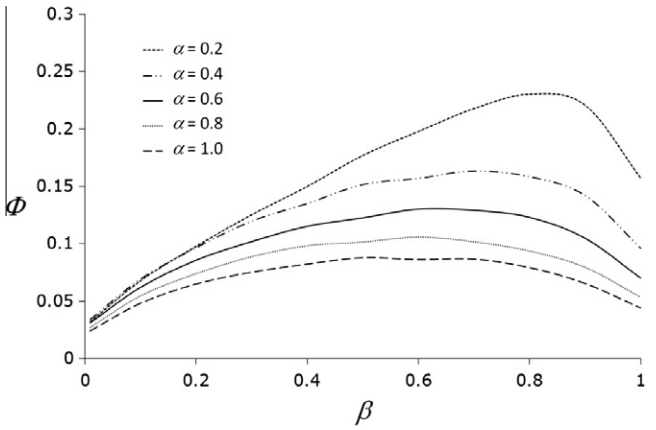

Fig. 9. Overall photonic efficiency for different values of α, β and $\rho = 0.4$ for the reactor configuration of 1 lamp.

By comparing Fig. 8b and c, it is possible to recognize that the in-line arrangement gives higher uniformity of the radiation distribution than the staggered one. This result is antagonist to the previous findings on photon absorption efficiency. As both performance indicators are equally important, the overall photonic efficiency Φ, which combines these two contrasting effects, allows the determination of the optimum design parameters.

In Fig. 9, the overall photonic efficiency Φ shows maxima when β is between 0.6 and 0.8, depending on the value of α. In order to have an optimal design, smaller values of α and β, which translate to a high catalytic surface area, are desirable. In the case of the reactor with one lamp, an optimum for α as a function of β can be calculated from:

$$\alpha_{Optimum} = 0.191\beta^2 - 0.5597\beta + 0.3854 \quad (9)$$

which was determined by plotting the locus of maxima of Φ as a function of β (Fig. 10). It should be noted that α decreases linearly until it reaches approximately $\beta = 0.7$. Thus, a lamp-diameter-to-plate-height ratio of 0.7 would be recommendable for optimum design when using one lamp.

Fig. 11 presents the result of the overall photonic efficiency for the reactor configurations with 4 and 5 lamps. Even though little differences can be observed in the behavior of these two arrangements, the in-line configuration (4 lamps) shows slightly higher overall photonic efficiency at the lowest values of α. Therefore, in-line arrangements would be advisable when using square plates (as used in this study). Nevertheless, staggered arrangements should not be disregarded; this configuration could be particularly

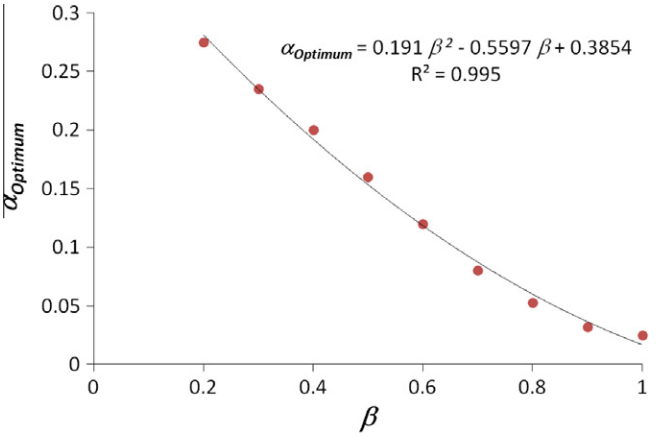

Fig. 10. Optimum plate-spacing-to-plate-height-ratio for the reactor configuration of one lamp.

advantageous if using rectangular plates. It also gives more flexibility on the number of lamps that can be utilized. Ideally, lamps should be equally spaced to have an efficient irradiation of the photocatalytic surface. But as it was observed in Fig. 11b, the irregular spacing between the lamps found in the configuration with 5 lamps had little effect on the overall photonic efficiency.

Fig. 12 shows the locus of the maxima of Φ for different α and β' for 4, 5 and 9 lamps configuration. The results can be fitted by a single correlation:

$$\alpha_{Optimum} = 0.3132\beta'^2 - 0.6238\beta' + 0.3073 \quad (10)$$

which gives a precise criteria for selecting the optimum geometrical design parameters for the MPPR. In all cases α decreases linearly until $\beta' = 0.5$. From this point, increasing the diameter of the lamp, which in turn, lessens the photocatalytic surface area, causes small reductions on the space between plates. Thus, this value should be considered to be the optimum β' and it should be used as a guide for selecting the appropriate number of lamps.

When designing a photoreactor, the length and diameter of the lamps will be constrained to the dimensions commercially available. Similarly, the size of the plates and reactor will be defined by the space limitations of the application. The optimum number of lamps can be calculated using the following formula:

$$N_{L\ optimum}^{1/2} = \frac{\beta'_{optimum}}{\beta} \quad (11)$$

By substituting the optimum β' with 0.5 (optimum found), the final equation would be:

$$N_{L\ optimum}^{1/2} = \frac{1}{2\beta} \quad (12)$$

Once the number of lamps has been selected, Eq. (10) will serve to define the optimum space between plates, which will ultimately determine the number of plates in the reactor.

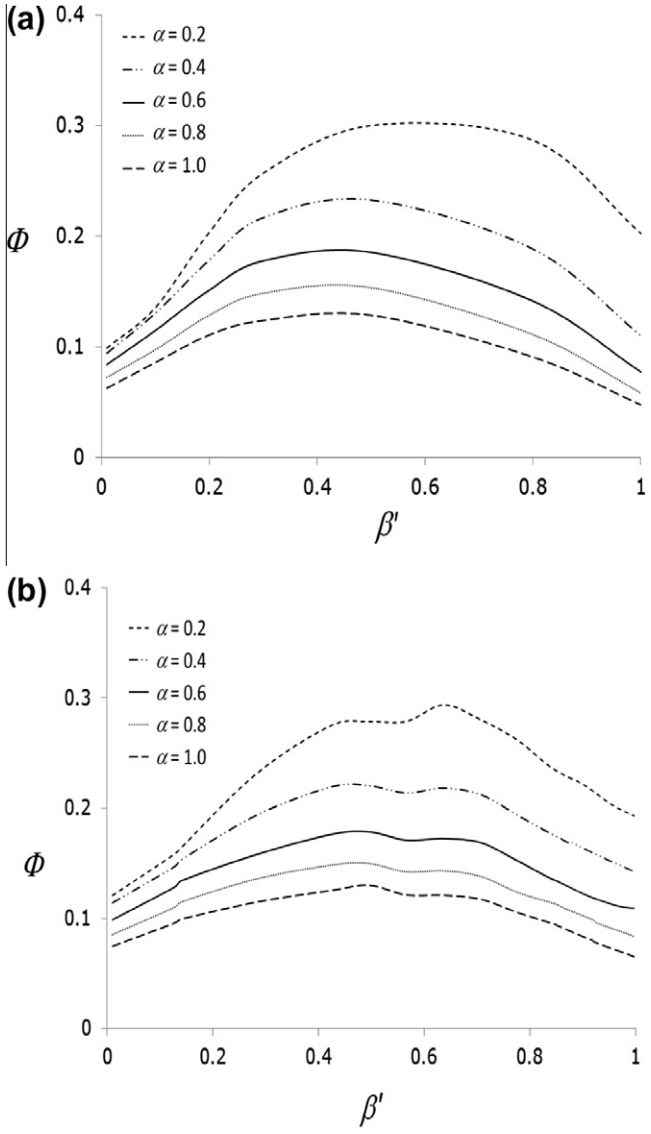

Fig. 11. Influence of α and β on the overall photonic efficiency for the reactor configuration with (a) 4 lamps and (b) 5 lamps. $\rho = 0.4$.

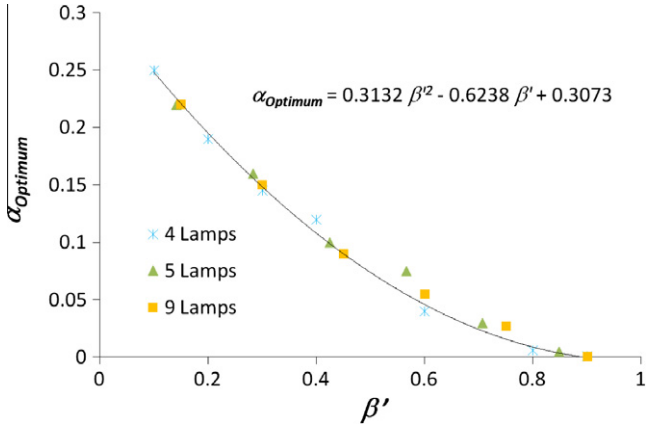

Fig. 12. Optimum plate-spacing-to-plate-height-ratio for the reactor configuration of 4, 5 and 9 lamps.

5.3. Experimental validation of model and apparent quantum yield

The apparent quantum yield for the oxidation of toluene in the MPPR was estimated from [26]:

$$\Phi_{app}(\%) = \frac{r_o W_{cat} N_A h c}{\lambda Q} \times 100 \quad (13)$$

where W_{cat} is the total weight of catalyst used (g); N_A is Avogadro's number (6.023×10^{23} molecules mol^{-1}); h is the Plank's constant (6.62×10^{-34} J s); c is the speed of light in a vacuum (2.997×10^{10} - cm s^{-1}); λ is the wavelength (m); Q is the radiant power reaching the photocatalytic plates in the reactor (W); r_o is the initial reaction rate based on a pseudo first order kinetic model (mol $gcat^{-1}$ s^{-1}). The corresponding kinetic constants were obtained from the slope of the line formed when the Neperian logarithm of the concentration of toluene is plotted versus time for each individual run.

Fig. 13 shows the apparent quantum yield calculated from Eq. (13) in eight photocatalytic experiments as a function of the geometrical parameter α, when five lamps and two photocatalytic plates were used with $\beta' = 0.3328$. Two photocatalytic plates were used here only for the purpose of validating the proposed model, although it is clear that this configuration does not represent an optimal design of the MPPR. A maximum in the apparent quantum yield was reached at $\alpha = 0.137$ which agreed very closely with the model prediction ($\alpha = 0.135$ from Eq. (10)). At smaller values of α the quantum yield is low because of poor distribution of radiation η over the surface of the plate. At higher values of α the quantum yield also decreases because of losses of photons (low ϕ) from the wide spacing between the catalytic plates. Then the quantum yield appears to plateau. In this operating region the spacing between the plates widens. In consequence, a larger volume of contaminated air is able to reach the catalytic surface by

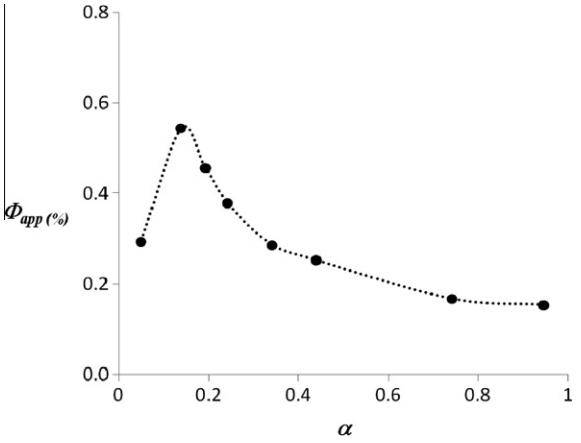

Fig. 13. Apparent quantum yield for the oxidation of toluene in the MPPR with two TiO_2-coated plates (one side irradiated on each plate) and 5 lamps, $\beta' = 0.3328$. The experimental error of the data point varied between 0.004 and 0.01.

transversal diffusional and convective transport. This increases the interchange of molecules at the catalytic surface increasing the overall removal rate of toluene, however, this effect is mitigated by lower radiation intensities at the photocatalytic surface which reduces the degradation rate. The results presented provide an experimental validation of the quantitative analysis of the MPPR presented in this study.

6. Conclusions

In this paper, the radiation field in a multi-plate photocatalytic reactor was investigated and successfully optimized by the Monte Carlo algorithm.

The results obtained for a reactor configuration with one lamp showed that the optimum lamp-diameter-to-plate height ratio should be 0.7 and that the optimum space-between-plates-to-plate-height ratio can be calculated by the equation: $[\alpha_{Optimum} = 0.191\,\beta^2 - 0.5597\,\beta + 0.3854]$. A multi-lamp reactor configuration allows the use of higher number of plates which in turn increases the total photocatalytic surface in the reactor. In such cases, the optimum β' for a multi-lamp arrangement was found to be approximately 0.5 and the optimum α for any given β' was defined by the correlation: $\alpha_{Optimum} = 0.3132\,\beta'^2 - 0.6238\,\beta' + 0.3073$.

It was noted that the in-line arrangement of lamps gives a slightly higher overall photonic efficiency compared to the staggered arrangement. This implies that the in-line arrangement results in a higher uniformity of the radiation distribution. However, this result is valid for the case of small square plates only. Staggered arrangements should be more suitable for larger square or rectangular photocatalytic plates. In these cases the lamps when positioned in equilateral triangular arrays (which represents equal distances between centerlines of lamps) should give maximum overall photonic efficiency.

Experiments of toluene oxidation validated the model predictions for optimal design.

Even though this quantitative study of the radiation field in the MPPR gave crucial insights for its optimum design other factors such as pressure drop, hydrodynamics, flow regimes (laminar or turbulent), reactant concentration and diffusional effects and cost need to be considered for the further optimization. Particularly, for the calculation of the optimum number of lamps, as this is a crucial design parameter that ultimately determines the operating costs of the reactor.

The dimensionless parametric optimization approach presented here could be used for the optimization of other reactor designs for the treatment of contaminated air or water streams.

Acknowledgments

The authors are grateful to NATO (Grant CPB.EAP.SFPP 982835), to The University of Nottingham (KTI: Knowledge Transfer Innovation Awards, KT052) and to CONACYT (PhD scholarship) for financial support.

References

[1] L.A. Wallace, E.D. Pellizzari, T.D. Hartwell, R. Whitmore, C. Sparacino, H. Zelon, Total exposure assessment methodology (team) study: Personal exposures, indoor–outdoor relationships, and breath levels of volatile organic compounds in New Jersey, Environ. Int. 12 (1986) 369–387.
[2] H. Destaillats, R.L. Maddalena, B.C. Singer, A.T. Hodgson, T.E. McKone, Indoor pollutants emitted by office equipment: a review of reported data and information needs, Atmos. Environ. 42 (2008) 1371–1388.
[3] W.J. Fisk, Health and productivity gains from better indoor environments and their relationship with building energy, Annu. Rev. Energy Environ. 25 (2000) 537–566.
[4] W.J. Fisk, A.H. Rosenfeld, Estimates of improved productivity and health from better indoor environments, Indoor Air 7 (1997) 158–172.
[5] W.A. Jacoby, D.M. Blake, R.D. Noble, C.A. Koval, Kinetics of the oxidation of trichloroethylene in air via heterogeneous photocatalysis, J. Catal. 157 (1995) 87–96.
[6] S.A. Larson, J.A. Widegren, J.L. Falconer, Transient studies of 2-propanol photocatalytic oxidation on titania, J. Catal. 157 (1995) 611–625.
[7] C.R. Esterkin, A.C. Negro, O.M. Alfano, A.E. Cassano, Air pollution remediation in a fixed bed photocatalytic reactor coated with TiO_2, AIChE J. 51 (2005) 2298–2310.
[8] O.-H. Park, H.-Y. Na, Photocatalytic degradation of toluene vapour using fixed bed multichannel photoreactors equipped with TiO_2 coated fabrics, Environ. Technol. 29 (2008) 1001–1007.
[9] I. Salvadó-Estivill, D.M. Hargreaves, G. Li Puma, Evaluation of the intrinsic photocatalytic oxidation kinetics of indoor air pollutants, Environ. Sci. Technol. 41 (2007) 2028–2035.
[10] M. Mohseni, F. Taghipour, Experimental and CFD analysis of photocatalytic gas phase vinyl chloride (VC) oxidation, Chem. Eng. Sci. 59 (2004) 1601–1609.
[11] T.N. Obee, Photooxidation of sub-parts-per-million toluene and formaldehyde levels on titania using a glass-plate reactor, Environ. Sci. Technol. 30 (1996) 3578–3584.
[12] L.A. Dibble, G.B. Raupp, Fluidized-bed photocatalytic oxidation of trichloroethylene in contaminated air streams, Environ. Sci. Technol. 26 (1992) 492–495.
[13] M. Zhang, T. An, J. Fu, G. Sheng, X. Wang, X. Hu, X. Ding, Photocatalytic degradation of mixed gaseous carbonyl compounds at low level on adsorptive TiO_2/SiO_2 photocatalyst using a fluidized bed reactor, Chemosphere 64 (2006) 423–431.
[14] M.M. Hossain, G.B. Raupp, S.O. Hay, T.N. Obee, Three-dimensional developing flow model for photocatalytic monolith reactors, AIChE J. 45 (1999) 1309–1321.
[15] J. Taranto, D. Frochot, P. Pichat, Photocatalytic air purification: comparative efficacy and pressure drop of a TiO_2-coated thin mesh and a honeycomb monolith at high air velocities using a 0.4 m^3 close-loop reactor, Sep. Purif. Technol. 67 (2009) 187–193.
[16] W. Choi, J.Y. Ko, H. Park, J.S. Chung, Investigation on TiO_2-coated optical fibers for gas-phase photocatalytic oxidation of acetone, Appl. Catal. B: Environ. 31 (2001) 209–220.
[17] F. Denny, J. Scott, G.-D. Peng, R. Amal, Channelled optical fibre photoreactor for improved air quality control, Chem. Eng. Sci. 65 (2010) 882–889.
[18] N.J. Peill, M.R. Hoffmann, Development and optimization of a TiO_2-coated fiber-optic cable reactor: photocatalytic degradation of 4-chlorophenol, Environ. Sci. Technol. 29 (1995) 2974–2981.
[19] S. Devahasdin, C. Fan, K. Li, D.H. Chen, TiO_2 photocatalytic oxidation of nitric oxide: transient behavior and reaction kinetics, J. Photochem. Photobiol. A 156 (2003) 161–170.
[20] T. Van Gerven, G. Mul, J. Moulijn, A. Stankiewicz, A review of intensification of photocatalytic processes, Chem. Eng. Process 46 (2007) 781–789.
[21] V. Pareek, S. Chong, M. Tadé, A.A. Adesina, Light intensity distribution in heterogenous photocatalytic reactors, Asia-Pac. J. Chem. Eng. 3 (2008) 171–201.
[22] M.K.H. Leung, S.M. Tang, R.C.W. Lam, D.Y.C. Leung, W.C. Yam, S.O. Ng, L.L.P. Vrijmoed, Parallel-plate solar photocatalytic reactor for air purification: Semi-empirical correlation, modeling, and optimization, Solar Energy 80 (2006) 949–955.

[23] H.A. Irazoqui, J. Cerdá, A.E. Cassano, Radiation profiles in an empty annular photoreactor with a source of finite spatial dimensions, AIChE J. 19 (1973) 460–467.
[24] A. Maudhuit, C. Raillard, V. Hequet, L. Le Coq, J. Sablayrolles, L. Molins, Adsorption phenomena in photocatalytic reactions: the case of toluene, acetone and heptanes, Chem. Eng. J. 170 (2011) 464–470.
[25] M. Singh, I. Salvadó-Estivill, G. Li Puma, Radiation field optimization in photocatalytic monolith reactors for air treatment, AIChE J. 53 (2007) 678–686.
[26] H. Ibrahim, H. de Lasa, Novel photocatalytic reactor for the destruction of airborne pollutants reaction kinetics and quantum yields, Ind. Eng. Chem. Res. 38–9 (1999) 3211–3217.